COBEM 2023 27TH INTERNATIONAL CONGRESS OF MECHANICAL ENGENEERING

ABCM Brazilian Society of Mechanical Sciences and Engineering
27th ABCM International Congress of Mechanical Engineering
December 04-08, 2023, Florianópolis-SC, Brazil

# COBEM2023-2196
# NUMERICAL SIMULATION OF COMPRESSIBLE AND INCOMPRESSIBLE NEWTONIAN FLOWS USING A TOTAL LAGRANGIAN POSITION-BASED FINITE ELEMENT FORMULATION

**Péricles R. P. Carvalho**
**Giovane Avancini**
**Rodolfo A. K. Sanches**
Department of Structural Engineering, São Carlos School of Engineering, University of São Paulo.
Av. Trab. São Carlense, 13566-590, São Carlos, São Paulo, Brazil
periclescarvalho@usp.br, giavancini@usp.br, rodolfo.sanches@usp.br

***Abstract.*** *We present a position-based finite element formulation for solving free-surface Newtonian fluid-flow problems using a total Lagrangian description. This formulation was already applied to incompressible Newtonian flows in previous works, and is extended to temperature-independent compressible cases in this work, allowing a comparison in terms of implementation and results, particularly for problems with moderate values of bulk modulus. To separate the volumetric and isochoric effects of the constitutive model, we apply the multiplicative decomposition of the deformation gradient. The employed approach differs from traditional fluid methods by using positions as nodal parameters of the system, instead of velocities. The compressible model has the advantage of not requiring additional pressure degrees of freedom in the global system. However, it can lead to numerical instabilities and convergence problems for large values of bulk modulus if no stabilization methods are applied. In order to evaluate the advantages and limitations of the model, a representative benchmark example is simulated, using different meshes and bulk modulus values. The obtained results are consistent, showing similarities between the compressible and incompressible models for moderate values of bulk modulus. However, to extend the formulation to quasi-incompressible models and allow larger values of bulk modulus without numerical instability issues, further implementations are required regarding numerical stabilization methods.*

***Keywords:*** *Fluid, Lagrangian, Compressible, Incompressible, Position-based, Finite Element Method*

## 1. INTRODUCTION

To this day, the simulation of free-surface fluid flows still presents challenges, and no computational method has superior capabilities over the others for all kinds of problems in this context. Well-established Eulerian formulations (Brooks and Hughes, 1982; Zienkiewicz and Taylor, 2000) are able to represent complex phenomena such as vortical structures, but are limited in regards to free-surface problems, needing additional techniques such as interface tracking and capturing. In this sense, strategies like the arbitrary Lagrangian-Eulerian method (Donea *et al.*, 1982; Sanches and Coda, 2014) are commonly applied, but still require advanced techniques for more complex situations.

Meanwhile, Lagrangian methods (Bach and Hassager, 1985; Ramaswamy and Kawahara, 1987) have the advantage of simpler formulations and more stable numerical implementations. That is because they eliminate the need for convective terms, since the mesh deforms together with the domain. This, however, prevents it from being used to problems with excessively large distortions or topological changes – such as vortical structures and joining/merging of subdomains –, unless a re-meshing technique is applied. In that sense, a method that has been widely regarded recently is the Particle Finite Element Method (Idelsohn *et al.*, 2004; Oñate *et al.*, 2014; Franci, 2016; Cremonesi *et al.*, 2020), which uses an updated Lagrangian description and velocity-based formulation, together with a robust re-meshing algorithm.

In Avancini and Sanches (2020), a total Lagrangian position-based Finite Element Formulation was proposed to simulate incompressible fluid flows. This formulation is simple, robust, and efficient for solving free-surface problems. Among other differences from velocity-based methods, it applies the incompressibility condition by imposing the volumetric strain as constant and unitary, instead of imposing the volumetric strain rate as null. Position-based formulations are also well-established in the nonlinear solid mechanics context, being applied successfully in works such as Coda and Paccola (2007, 2014); Carvalho *et al.* (2020).

In this work, we extend the formulation of Avancini and Sanches (2020) to compressible fluid flows, using a similar position-based Finite Element Framework. In this case, however, there are no incompressibility conditions, and no pressure parameters in the global system. Therefore, the formulation is purely position-based, instead of mixed position-pressure. While compressible or quasi-incompressible fluid models have already been applied in velocity-based formulations (Oñate *et al.*, 2014; Franci, 2016), the present position-based method allows the constitutive model to derive from a direct relation between pressures and volumetric strains, instead of pressure rates and volumetric strain rates. Addition-

ally, we make use of the multiplicative decomposition of the deformation gradient to properly separate the volumetric and isochoric effects, further improving the theoretical approach and mathematical description of the model.

As a Lagrangian method, the present formulation is applied to free-surface fluid-flows with finite domains. More specifically, this work is focused on adiabatic problems without vortical structures (small Reynolds numbers), allowing the use of a standard Finite Element mesh to accommodate domain distortions without the need for remeshing techniques. For using the FEM as a basis, the present formulation dispenses the use of a grid for domain discretization, and allows for unstructured meshes.

## 2. NEWTONIAN FLUID MODEL

To describe the motion of the domain, we employ the continuum hypothesis. Let $\mathbf{y}$ denote the current/deformed positions of a body, and $\mathbf{x}$ the initial/undeformed positions. We define the deformation gradient as $\mathbf{F} = \boldsymbol{\nabla}_{\mathbf{x}}\, \mathbf{y}$, where $\boldsymbol{\nabla}_{\mathbf{x}}$ is the gradient with respect to the initial configuration. Then, we can define the right Cauchy-Green stretch as

$$\mathbf{C} = \mathbf{F}^T\mathbf{F}, \tag{1}$$

the Jacobian, or volumetric strain, as

$$J = \det \mathbf{F}, \tag{2}$$

and the infinitesimal strain rate as

$$\mathbf{D} = \frac{1}{2}\left(\boldsymbol{\nabla}_{\mathbf{y}}\, \dot{\mathbf{y}} + \boldsymbol{\nabla}_{\mathbf{y}}^T\, \dot{\mathbf{y}}\right) = \frac{1}{2}\left(\dot{\mathbf{F}}\mathbf{F}^{-1} + \mathbf{F}^{-T}\dot{\mathbf{F}}^T\right), \tag{3}$$

where $\boldsymbol{\nabla}_{\mathbf{y}}$ is the gradient with respect to the current configuration, and $\dot{(\,)}$ denotes the time derivative. After certain algebraic manipulations, it is possible to show that the engineering strain rate can be related to the right Cauchy-Green stretch rate by the following expression:

$$\dot{\mathbf{C}} = 2\mathbf{F}^T\mathbf{D}\mathbf{F}. \tag{4}$$

For compressible materials, where both volumetric and isochoric strains are involved, it is convenient to decompose the deformation gradient in the form $\mathbf{F} = \hat{\mathbf{F}}\bar{\mathbf{F}}$, where $\hat{\mathbf{F}}$ represents the volumetric part of the deformation gradient, and $\bar{\mathbf{F}}$ the isochoric one. In order to properly separate the effects, it is necessary that $\hat{\mathbf{F}}$ encompasses all volumetric strain, that is, $\hat{J} = \det\hat{\mathbf{F}} = J$ and $\bar{J} = \det\bar{\mathbf{F}} = 1$. This can be achieved by making $\hat{\mathbf{F}} = J^{1/3}\mathbf{I}$, where $\mathbf{I}$ is the identity tensor. Therefore, we have

$$\mathbf{F} = J^{1/3}\bar{\mathbf{F}} \qquad \text{or} \qquad \bar{\mathbf{F}} = J^{-1/3}\mathbf{F}. \tag{5}$$

Consequently,

$$\bar{\mathbf{C}} = \bar{\mathbf{F}}^T\bar{\mathbf{F}} = J^{-2/3}\mathbf{F}^T\mathbf{F} = J^{-2/3}\mathbf{C}, \tag{6}$$

$$\dot{\bar{\mathbf{F}}} = J^{-1/3}\left[\dot{\mathbf{F}} - \frac{1}{3}\text{tr}(\dot{\mathbf{F}}\mathbf{F}^{-1})\mathbf{F}\right], \quad \text{and} \tag{7}$$

$$\dot{\bar{\mathbf{C}}} = J^{-2/3}\left[\dot{\mathbf{C}} - \frac{1}{3}\text{tr}(\dot{\mathbf{C}}\mathbf{C}^{-1})\mathbf{C}\right]. \tag{8}$$

where $\text{tr}(\cdot)$ denotes the trace of a tensor. Furthermore, using the previous equations, it is possible to show that

$$\bar{\mathbf{D}} = \frac{1}{2}\left(\dot{\bar{\mathbf{F}}}\bar{\mathbf{F}}^{-1} + \bar{\mathbf{F}}^{-T}\dot{\bar{\mathbf{F}}}^T\right) = \frac{1}{2}\bar{\mathbf{F}}^{-T}\dot{\bar{\mathbf{C}}}\bar{\mathbf{F}}^{-1} = \mathbf{D} - \frac{1}{3}\text{tr}(\mathbf{D})\mathbf{I} = \text{dev}(\mathbf{D}), \tag{9}$$

where $\text{dev}(\cdot)$ denotes the deviatoric part of a tensor.

From an Eulerian perspective, the newtonian fluid model applied in this work can be written as

$$\boldsymbol{\sigma} = p\mathbf{I} + 2\mu\bar{\mathbf{D}}, \tag{10}$$

where $\boldsymbol{\sigma}$ is the Cauchy stress, $p$ is the pressure, and $\mu$ is the fluid viscosity. As can be seen, the Cauchy stress is composed of a pressure-dependent (volumetric) part, and a viscous (isochoric) part. For incompressible materials, the viscous part can be written simply in terms of $\mathbf{D}$ (Avancini and Sanches, 2020), as we have $J = 1$, $\mathbf{F} = \bar{\mathbf{F}}$ and, consequently, $\mathbf{D} = \bar{\mathbf{D}}$. However, since we also consider compressible models in this work, we write the viscous part only in terms of the isochoric strain components, i.e. we apply $\bar{\mathbf{D}}$ instead of $\mathbf{D}$.

From Eq. (9), we concluded that $\bar{\mathbf{D}}$ is purely deviatoric, and, therefore, so is the viscous part of the Cauchy stress. As such, we have $\text{tr}(\boldsymbol{\sigma}) = \text{tr}(p\mathbf{I}) = p$, that is, the hydrostatic/volumetric effect of the constitutive model is solely represented by the pressure, as it should be. This would not be true for compressible models with viscous part written in terms of $\mathbf{D}$.

In order to use a total Lagrangian framework, we write the constitutive model in terms of the second Piola-Kirchhoff stress, denoted by $\mathbf{S}$. Using the well-known relation $\mathbf{S} = J\mathbf{F}^{-1}\boldsymbol{\sigma}\mathbf{F}^{-T}$, as well as Eqs. (1), (5) and (9), we can write:

$$\mathbf{S} = pJ\mathbf{F}^{-1}\mathbf{F}^{-T} + \mu J\mathbf{F}^{-1}\bar{\mathbf{F}}^{-T}\dot{\bar{\mathbf{C}}}\bar{\mathbf{F}}^{-1}\mathbf{F}^{-T} = pJ\mathbf{C}^{-1} + \mu J^{5/3}\mathbf{C}^{-1}\dot{\bar{\mathbf{C}}}\mathbf{C}^{-1}. \tag{11}$$

Then, applying Eq. (8) and performing further algebraic manipulations,

$$\mathbf{S} = pJ\mathbf{C}^{-1} + \mu J\ \text{dev}(\mathbf{C}^{-1}\dot{\mathbf{C}})\mathbf{C}^{-1} \qquad \text{or} \qquad \mathbf{S} = pJ\mathbf{C}^{-1} + \frac{1}{2}\mathcal{D} : \dot{\mathbf{C}}, \tag{12}$$

where the operator ":" denotes a double contraction, and $\mathcal{D}$ is the fourth-order viscosity operator, defined as

$$\mathcal{D}_{ijkl} = 2\mu J\left(C^{-1}_{ik}C^{-1}_{jl} - \frac{1}{3}C^{-1}_{ij}C^{-1}_{kl}\right). \tag{13}$$

To conclude the constitutive model definition, we must determine how the volumetric part is treated. For incompressible flows, the pressures are calculated as unknown variables of the global system, by imposing additional incompressibility conditions. For the compressible model applied in this work, we define the pressure directly by the expression

$$p = \frac{\Lambda}{J}\ln J, \tag{14}$$

where $\Lambda$ is the bulk modulus of the material. Mathematically speaking, the presented compressible model is associated with the penalty method, while the incompressible model is associated with the Lagrange multiplier method. Therefore, in theory, both should coincide approximately for higher values of penalty parameter (in this case, $\Lambda$). However, in practice, high values of $\Lambda$ could lead to ill conditioned systems, leading to numerical issues and inaccuracies if not treated correctly with stabilization methods. When these methods are taken into account, one could represent the so-called quasi-incompressible flows (Franci, 2016), which are not within the scope of this work.

## 3. POSITION-BASED FINITE ELEMENT METHOD

Following standard finite element procedures, we discretize the domain into a mesh of finite elements, with a given number of nodes and order of shape functions. By making use of an auxiliary finite element defined in parametric coordinates $\boldsymbol{\xi}$, the current and initial positions in an element can be interpolated using the following expressions, respectively:

$$\mathbf{y}(\boldsymbol{\xi}) = \varphi_\alpha(\boldsymbol{\xi})\mathbf{y}_\alpha \qquad \text{and} \qquad \mathbf{x}(\boldsymbol{\xi}) = \varphi_\alpha(\boldsymbol{\xi})\mathbf{x}_\alpha, \tag{15}$$

where $\mathbf{y}_\alpha$ and $\mathbf{x}_\alpha$ are the current and initial positions of each node $\alpha$, respectively, and $\varphi_\alpha$ is the shape function of $\alpha$, defined in the parametric domain of the auxiliary finite element. Then, we can calculate the deformation gradient as

$$\mathbf{F} = \boldsymbol{\nabla}_{\mathbf{x}}\,\mathbf{y} = \frac{\partial \mathbf{y}}{\partial \mathbf{x}} = \frac{\partial \mathbf{y}}{\partial \boldsymbol{\xi}}\left(\frac{\partial \mathbf{x}}{\partial \boldsymbol{\xi}}\right)^{-1} = \mathbf{F}_1\mathbf{F}_0^{-1} \tag{16}$$

where $\mathbf{F}_1$ and $\mathbf{F}_0$ are the deformation gradients from the parametric finite element domain to the current and initial domains, respectively, calculated as

$$\mathbf{F}_1 = \frac{\partial \mathbf{y}}{\partial \boldsymbol{\xi}} = \mathbf{y}_\alpha \otimes \frac{\partial \varphi_\alpha}{\partial \boldsymbol{\xi}} \qquad \text{and} \qquad \mathbf{F}_0 = \frac{\partial \mathbf{x}}{\partial \boldsymbol{\xi}} = \mathbf{x}_\alpha \otimes \frac{\partial \varphi_\alpha}{\partial \boldsymbol{\xi}}. \tag{17}$$

Similarly, we can obtain the rate of deformation gradient as

$$\dot{\mathbf{F}} = \dot{\mathbf{F}}_1\mathbf{F}_0^{-1}, \qquad \text{where} \qquad \dot{\mathbf{F}}_1 = \dot{\mathbf{y}}_\alpha \otimes \frac{\partial \varphi_\alpha}{\partial \boldsymbol{\xi}}. \tag{18}$$

Then, using Eqs. (1) and (12), one can calculate the right Cauchy-Green stretch, as well as its rate, and the second Piola-Kirchhoff stress, which are directly applied into the mechanical problem.

In summary, the transient mechanical problem consists in solving the following equilibrium equation, written in global variational form, using a total Lagrangian description:

$$\int_{\Omega_0}\left(\frac{1}{2}\,\mathbf{S} : \delta\mathbf{C} + \rho_0\ddot{\mathbf{y}}\cdot\delta\mathbf{y} - \mathbf{b}\cdot\delta\mathbf{y}\right)\,dV_0 = 0, \tag{19}$$

where $\Omega_0$ and $V_0$ are the initial domain and volume, respectively, $\rho_0$ is the initial specific mass, $\mathbf{b}$ is the prescribed volume force, and $\delta$ denotes a variation applied on a given variable. For simplicity, we chose to conceal the component of boundary forces, as they are not applied in the numerical example of Sec. 4.1 Applying Galerkin method in Eq. (19), i.e. assuming that $\delta\mathbf{y} = \varphi_\alpha \delta\mathbf{y}_\alpha$, and using the arbitrariness of the nodal variations $\delta\mathbf{y}_\alpha$, we have the following equilibrium equation for each node $\alpha$:

$$\frac{1}{2}\int_{\Omega_0} \mathbf{S} : \frac{\partial \mathbf{C}}{\partial \mathbf{y}_\alpha}\, dV_0 + \int_{\Omega_0} \rho_0 \varphi_\alpha \varphi_\beta \ddot{\mathbf{y}}_\alpha \, dV_0 - \int_{\Omega_0} \varphi_\alpha \mathbf{b}\, dV_0 = 0, \tag{20}$$

where the three components represent, respectively, the internal force, the kinetic force, and the volume force applied at node $\alpha$. For the numerical integration, we apply Newmark-$\beta$ method, where the current velocities ($\dot{\mathbf{y}}$) and accelerations ($\ddot{\mathbf{y}}$) in each node are calculated using the following equations as basis:

$$\mathbf{y} = \mathbf{y}_s + \dot{\mathbf{y}}_s \Delta t + \left[(1-2\beta)\,\ddot{\mathbf{y}}_s + 2\beta \ddot{\mathbf{y}}\right]\frac{\Delta t^2}{2}, \qquad \text{and} \tag{21}$$

$$\dot{\mathbf{y}} = \dot{\mathbf{y}}_s + (1-\gamma)\Delta t \ddot{\mathbf{y}}_s + \gamma \Delta t \ddot{\mathbf{y}}, \tag{22}$$

in which $\beta$ and $\gamma$ are the newmark parameters, and the index $(\cdot)_s$ indicates a variable taken from the previous time step. With that, Eq. (20) is written entirely in terms of the nodal positions.

For incompressible cases, additional pressure parameters are added as unknowns of the system, together with additional equations known as incompressibility conditions. Further details are discussed in Avancini and Sanches (2020), including the strategy used for numerical stabilization in this case.

## 4. NUMERICAL IMPLEMENTATION

The present formulation is implemented into an in-house software using C++ language. To solve Eq. (20) for the current positions ($\mathbf{y}$), we apply the Newton-Raphson method, with stopping criterion for convergence set at $\|\Delta\mathbf{y}\|/\|\Delta\mathbf{x}\| \leq 10^{-6}$, where $\Delta\mathbf{y}$ is the variation of positions between current and previous algorithm iterations. To solve the global system of equations at each iteration, the PETSc library is employed.

### 4.1 EXAMPLE: DAM BREAK OVER A SLIP FLAT SURFACE

To showcase the proposed model, we simulate a classical benchmark example for free-surface fluid problems. We consider a water column subject to its self weight, with geometry, boundary conditions, and parameters presented in Fig. 1. In addition to the incompressible model, used for reference, we apply compressible models with 4 different values of $\Lambda$: $10^0$, $10^1$, $10^2$ and $10^3$ MPa. In order to dissipate the high frequencies for this problem, we use the Newmark-$\beta$ parameters from Hu (1997): $\beta = 1$ and $\gamma = 1.5$.

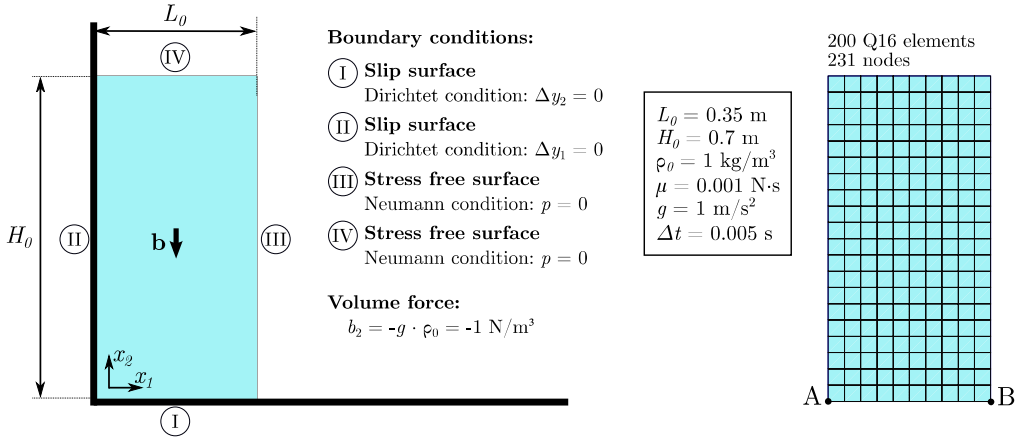


Figure 1. Geometry and parameters for the dam break example

Quadrilateral elements with 16 nodes and cubic approximation (Q16) are used. For a first analysis, a constant mesh with $10 \times 20$ elements and 231 nodes is applied, as shown in Fig. 1. The results of width variation, pressure at the bottom left corner (point A), total volume of the current domain, and number of Newton-Raphson iterations over time are shown in Fig. 2. The width variation is calculated as $L/L_0$, where $L_0$ is the original width (0.35 m) and $L$ is the current width (distance between points $A$ and $B$).

As can be seen, the width variation is only loosely dependent of the bulk modulus, assuming values relatively close to the incompressible case for almost all considered cases, except $\Lambda = 10^0$ MPa. This indicates that the displacement at

point B is more influenced by the viscous part of the constitutive model than the volumetric part. On the other hand, the volumetric-related variables, such as pressure and total volume, are more sensible to the bulk modulus, being closer to the incompressible case only for higher values of $\Lambda$. As expected from the elastic nature of the adopted compressible law, we can observe characteristic oscillatory behaviors in both variables, with frequency varying according to $\Lambda$.

Naturally, the total volume is constant for the incompressible model, and tends to be more stationary for higher values of bulk modulus, with notably good convergence (in practical terms) already for the case with $\Lambda = 10^2$ MPa. For the pressure, however, a sufficiently good convergence can be seen only for $\Lambda = 10^3$ MPa, as the case with $\Lambda = 10^2$ MPa still causes visible discordant oscillations at the beginning of the analysis, dissipated only after a certain time. Nonetheless, it must be noted that the increase of $\Lambda$ makes the system become more ill conditioned, which is translated into numerical instabilities, such as the increase of Newton-Raphson iterations. Indeed, as noted from Fig. 2(d), the number of iterations also highly increase with $\Lambda$, reaching abnormal values of almost 75 iterations for $\Lambda = 10^3$ MPa, and almost 30 iterations for $\Lambda = 10^2$ MPa.

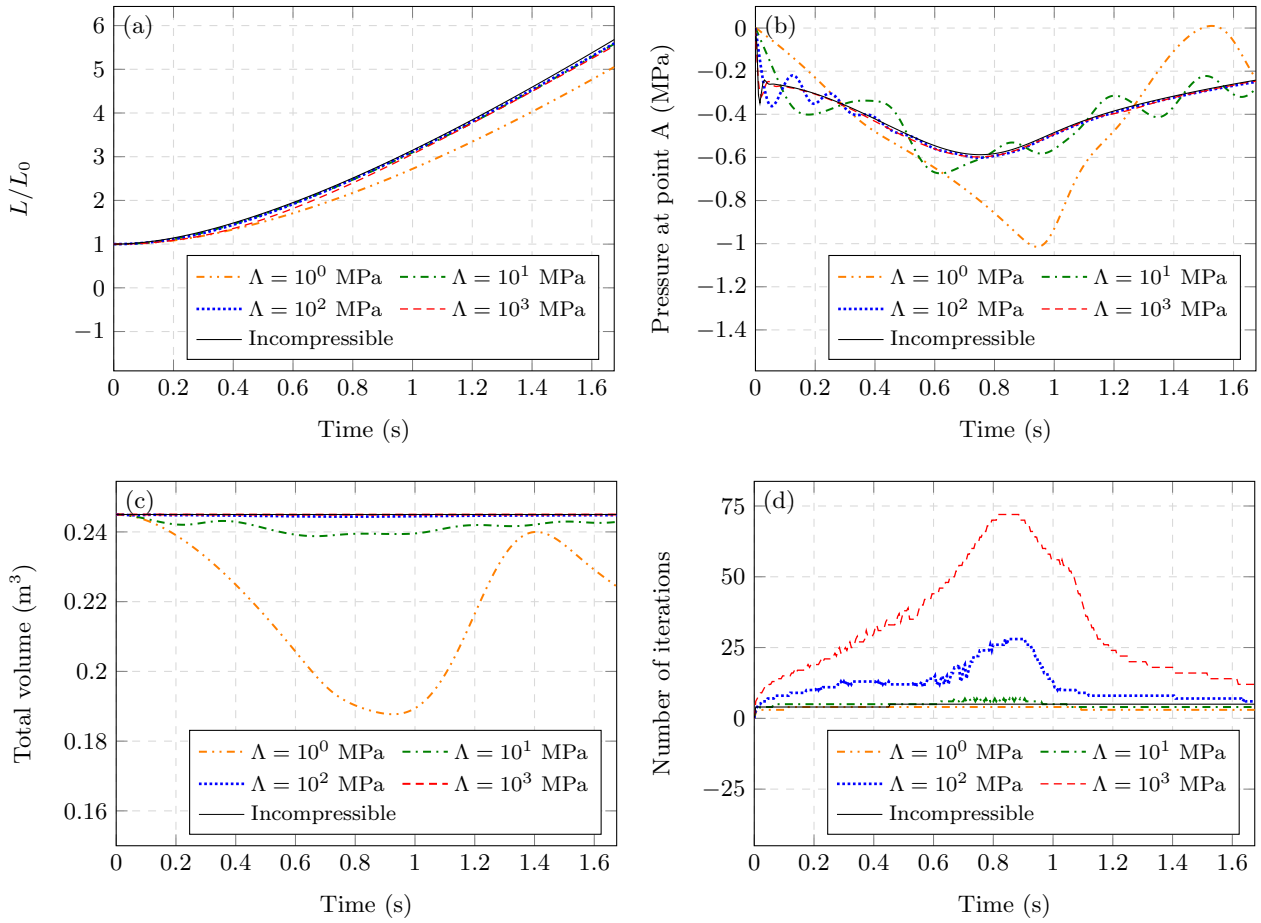


Figure 2. Dam break: comparison between incompressible and compressible models with different $\Lambda$ values, using a 10x10 mesh with Q16 elements.

The deformed configurations for each of the cases are shown in Figs. 3 to 7, with pressure displayed in color map. As can be seen, the numerical instabilities due to increased bulk modulus values reflect not only in the number of iterations, but also in the pressure distribution and overall deformed configuration. While the pressure specifically located at point A presents the already discussed behavior of Fig. 2(b), the color map show some unnatural spikes (both positive and negative) in other points. These spikes are more noticeable for greater values of bulk modulus, greatly undermining the overall view of the pressure map. Furthermore, some inconsistencies in the deformed configuration can be seen for greater $\Lambda$ values, specially at the elements with pressure spikes and the one containing point B. These problems, along with the convergence issues, indicate the need for stabilization methods when using the compressible model with high values of bulk modulus.

Following, we perform a mesh convergence analysis with h-refinement (i.e. keeping the Q16 element type). In Fig. 8, we present the results of width variation and pressure over time for different values of $\Lambda$ and meshes (4x8, 6x12, 8x16 and 10x20). As noted from Fig. 8(b), highest values of $\Lambda$ make the problem significantly more mesh dependent: for the case with $\Lambda = 10^1$ MPa, the influence of h-refinement on the pressure is barely noticeable. On the other side, for the

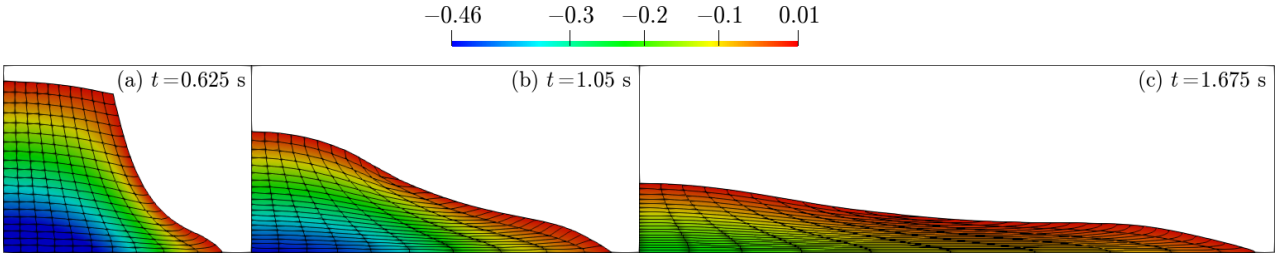


Figure 3. Dam break: deformed configurations and pressures for the incompressible model

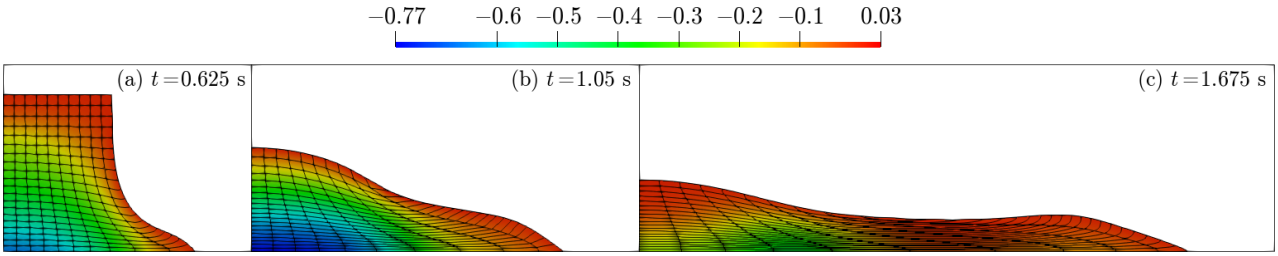


Figure 4. Dam break: deformed configurations and pressures for $\Lambda = 10^0$ MPa

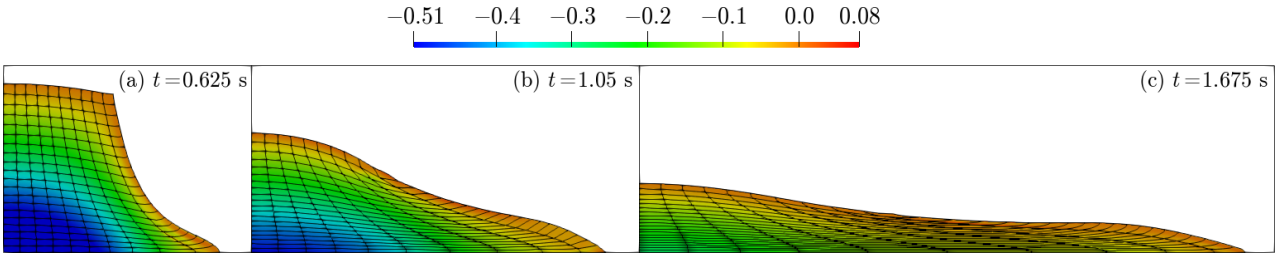


Figure 5. Dam break: deformed configurations and pressures for $\Lambda = 10^1$ MPa

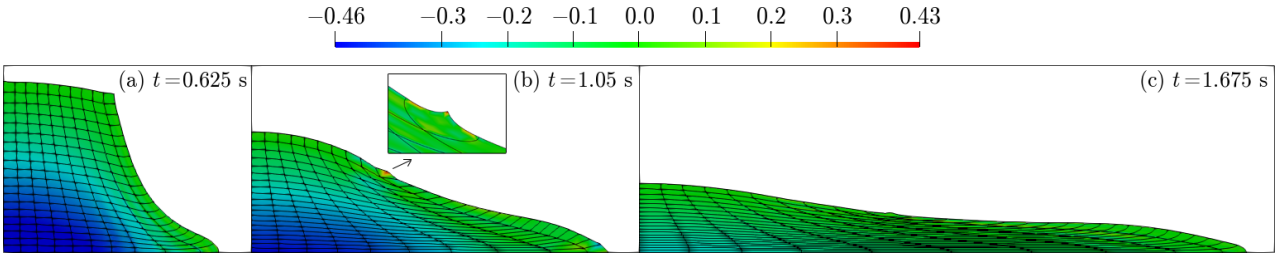


Figure 6. Dam break: deformed configurations and pressures for $\Lambda = 10^2$ MPa

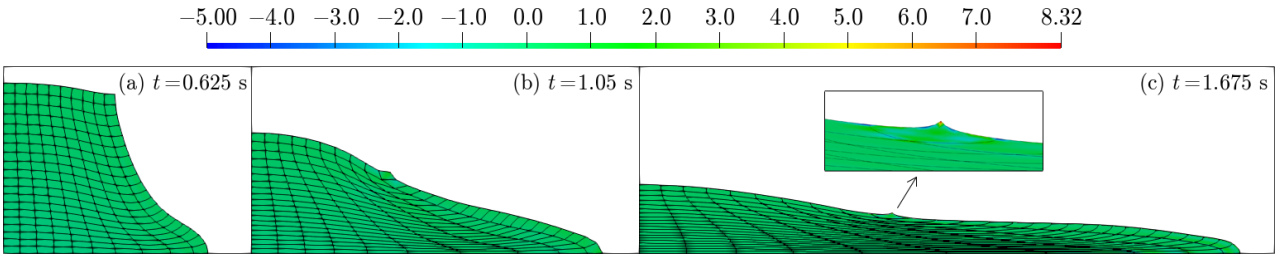


Figure 7. Dam break: deformed configurations and pressures for $\Lambda = 10^3$ MPa

case with $\Lambda = 10^3$ MPa, it can be seen that each mesh exhibits a distinct characteristic behavior, and a more visible convergence can only be noticed between the two most refined meshes, 8x8 and 10x10. This behavior is likely related to the aforementioned numerical instabilities of the compressible model with high values of $\Lambda$. However, this problem is only relevant for volumetric-related variables, such as the pressure. The width variation, for example, is more affected by the viscous part of the constitutive model, and therefore suffers minimal influence of mesh refinement, as seen in Fig. 8(a).

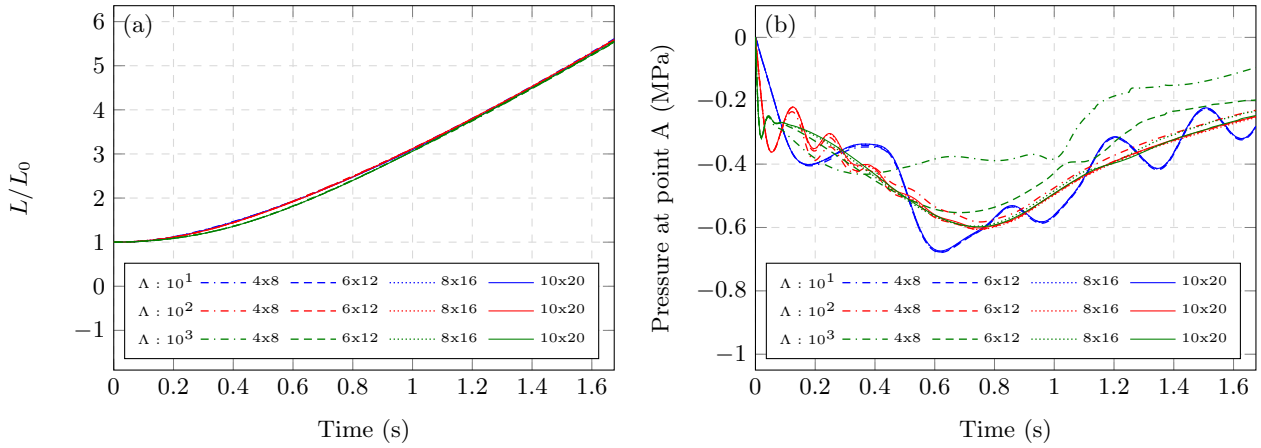


Figure 8. Dam break: influence of h-refinement using Q16 elements and different $\Lambda$ values.

## 5. CONCLUSIONS

The main contribution of this work is the extension of the position-based fluid formulation introduced by Avancini and Sanches (2020) to compressible flows, with the application of a multiplicative decomposition between volumetric and isochoric deformations. Similarly to the mentioned work, the formulation is able to solve free-surface fluid problems using a total Lagrangian formulation. However, the proposed model has the advantage of not requiring additional pressure degrees of freedom, narrowing greatly the size of the system, at the price of reducing the precision of the incompressibility conditions and having additional numerical considerations to be addressed, as discussed subsequently.

The model was applied to a free-surface problem where the viscosity effect is dominant over the volumetric. The obtained results are consistent, and show similarities between the compressible and incompressible models even for moderate values of bulk modulus. For higher values, however, the system becomes more ill conditioned, and some numerical instabilities arise, which causes convergence issues, pressure spikes, and overall inconsistencies.

To address this issue, future researches may consider enhancing the current model by implementing numerical stabilization methods, such as the one presented in Franci (2016). These methods allow the use of larger bulk modulus values (quasi-incompressible models) and the simulation of volumetric-dominant problems, significantly expanding the scope of applications for the proposed formulation.

## 6. ACKNOWLEDGEMENTS

This study was financed in part by the *Coordenação de Aperfeiçoamento de Pessoal de Nível Superior – Brasil* (CAPES) – Finance Code 001 –, the Brazilian agency National Council for Scientific and Technological Development (CNPq) – grant 310482/2016-0 –, and the São Paulo Research Foundation (FAPESP) – Process Number 2018/23957-2. The authors would like to thank them for the financial support given to this research.

## 7. REFERENCES

Avancini, G. and Sanches, R.A., 2020. "A total lagrangian position-based finite element formulation for free-surface incompressible flows". *Finite Elements in Analysis and Design*, Vol. 169, p. 103348. ISSN 0168-874X. doi: https://doi.org/10.1016/j.finel.2019.103348.

Bach, P. and Hassager, O., 1985. "An algorithm for the use of the lagrangian specification in newtonian fluid mechanics and applications to free-surface flow". *Journal of Fluid Mechanics*, Vol. 152, p. 173–190. doi: 10.1017/S0022112085000635.

Brooks, A.N. and Hughes, T.J., 1982. "Streamline upwind/petrov-galerkin formulations for convection dominated flows with particular emphasis on the incompressible navier-stokes equations". *Computer Methods in Applied Mechanics and Engineering*, Vol. 32, No. 1, pp. 199 – 259. ISSN 0045-7825. doi:https://doi.org/10.1016/0045-7825(82)90071-8.

Carvalho, P.R.P., Coda, H.B. and Sanches, R.A.K., 2020. "Positional finite element formulation for two-dimensional analysis of elasto-plastic solids with contact applied to cold forming processes simulation". *Journal of the Brazilian Society of Mechanical Sciences and Engineering*, Vol. 42, No. 5, p. 245. ISSN 1806-3691. doi:10.1007/s40430-020-02344-z.

Coda, H.B. and Paccola, R.R., 2007. "An alternative positional FEM formulation for geometrically non-linear analysis of shells: Curved triangular isoparametric elements". *Computational Mechanics*, Vol. 40, No. 1, pp. 185–200. ISSN

01787675. doi:10.1007/s00466-006-0094-1.

Coda, H.B. and Paccola, R.R., 2014. "A total-lagrangian position-based FEM applied to physical and geometrical nonlinear dynamics of plane frames including semi-rigid connections and progressive collapse". *Finite Elements in Analysis and Design*, Vol. 91, pp. 1–15. ISSN 0168874X. doi:10.1016/j.finel.2014.07.001.

Cremonesi, M., Franci, A., Idelsohn, S. and Oñate, E., 2020. "A state of the art review of the particle finite element method (pfem)". *Archives of Computational Methods in Engineering*, Vol. 27. doi:10.1007/s11831-020-09468-4.

Donea, J., Giuliani, S. and Halleux, J., 1982. "An arbitrary lagrangian-eulerian finite element method for transient dynamic fluid-structure interactions". *Computer Methods in Applied Mechanics and Engineering*, Vol. 33, No. 1, pp. 689–723. ISSN 0045-7825. doi:https://doi.org/10.1016/0045-7825(82)90128-1.

Franci, A., 2016. *Unified Lagrangian Formulation for Fluid and Solid Mechanics, Fluid-Structure Interaction and Coupled Thermal Problems Using the PFEM*. Springer Theses. Springer International Publishing. ISBN 9783319456614.

Hu, N., 1997. "A solution method for dynamic contact problems". Vol. 63, pp. 1053–1063.

Idelsohn, S., Oñate, E. and Pin, F.D., 2004. "The particle finite element method: a powerful tool to solve incompressible flows with free-surfaces and breaking waves". *International Journal for Numerical Methods in Engineering*, Vol. 61, No. 7, pp. 964–989. doi:10.1002/nme.1096.

Oñate, E., Franci, A. and Carbonell, J.M., 2014. "Lagrangian formulation for finite element analysis of quasi-incompressible fluids with reduced mass losses". *International Journal for Numerical Methods in Fluids*, Vol. 74, No. 10, pp. 699–731. doi:https://doi.org/10.1002/fld.3870.

Ramaswamy, B. and Kawahara, M., 1987. "Lagrangian finite element analysis applied to viscous free surface fluid flow". *International Journal for Numerical Methods in Fluids*, Vol. 7, No. 9, pp. 953–984. doi:https://doi.org/10.1002/fld.1650070906.

Sanches, R.A.K. and Coda, H.B., 2014. "On fluid–shell coupling using an arbitrary lagrangian–eulerian fluid solver coupled to a positional lagrangian shell solver". *Applied Mathematical Modelling*, Vol. 38, No. 14, pp. 3401 – 3418. ISSN 0307-904X.

Zienkiewicz, O. and Taylor, R., 2000. *The Finite Element Method: Fluid dynamics*. The Finite Element Method. Butterworth-Heinemann. ISBN 9780340759837.

## 8. RESPONSIBILITY NOTICE

The authors are solely responsible for the printed material included in this paper.